Proceedings of the 34th Annual Cement and Concrete Science Conference, and Workshop on Waste Cementation

14 – 17 September 2014

Editors
Susan A. Bernal & John L. Provis

The Institute of Materials, Minerals and Mining

Table of contents

34th Conference on Cement and Concrete Science – 14-16 Sep 2014

Oral Sessions - Extended Abstracts

		Pages
	Keynotes	
K1	Professor Fredrik Glasser	1
K2	Dr Andrea Hamilton	3
K3	Professor Robert Flatt	7
K4	Dr Nicolas Roussel	11
K5	Professor Andrey Kalinichev	13
	Contributed lectures	
	Sustainability	
A1	Reducing CO_2: Optimum Blend of Binders in the UK *A.C. Heath, K.A. Paine*	15
A2	The Design of Concrete Mixes with Reduced Clinker Content *G.W. Nganga, M.G. Alexander, H.D. Beushausen*	19
A3	Towards Carbon Negative Cements *J. Morrison, G. Jauffret, F.P. Glasser, J.L. Galvez-Martos, M.S. Imbabi*	23
	Alkali-Activation	
B1	Stoichiometrically Controlled C-A-S-H/N-A-S-H Gel Blends via Alkali-Activation of Synthetic Precursors *B. Walkley, J.S.J van Deventer, R. San Nicolas, J.L. Provis*	27
B2	Effect of NaOH Concentration and Silica Fume Addition on Strength and Durability of Geopolymer Cements *S. Astutiningsih, H.O. Adriansyah*	33
B3	Structural Investigations on One-Part Geopolymers after Different Drying Regimes *P. Sturm, G.J.G. Gluth, M. Lindemann, S. Greiser, C. Jäger, H.J.H. Brouwers*	37
B4	Steel Reinforced Geopolymer Mortar: Corrosion Behaviour in Chloride-Rich Environment *M.E. Natali, S. Manzi, C. Chiavari, M.C. Bignozzi, C. Monticelli, M. Abbottoni, A. Balbo, F. Zanotto*	41
B5	Manufacturing Cement-based Materials and Building Products via Extrusion *X.M. Zhou, Z.J. Li*	45
B6	Alkaline Activation of Natural Iron Containing Precursors *K.C. Gomes, J.F. Silva Neto, M.R.F. Lima Filho, Gomes, R.M., S.M. Torres, A.A.P. Vieira*	49

B7	Active Steel Corrosion in Blended Slag and Fly Ash Geopolymer Concrete *M. Babaee, A. Castel, A. Akbarnezhad*	55
B8	Drying Shrinkage Microcracking of Alkali-Activated Slag Materials *S.A. Bernal, J. Bisschop, J.S.J. van Deventer, J.L. Provis*	59

Composites and Lightweight Materials

C1	Effect of Additives on Void Structure of Foamed Concrete *A.A. Hilal, N.H. Thom, A.R. Dawson*	63
C2	Cumulative Pore Volume and Pore Size Distribution of Porous Inorganic Polymer Composites: Relation Microstructure and Effective Thermal Conductivity *Z.N.M. NGouloure, E. Kamseu, U.C. Melo, C. Leonelli, B. Nait-Ali, D.S. Rossignol, S. Zekeng*	67
C3	Microstructural Study of 10-year Aged GRC Modified by Calcium Sulfoaluminate Cement *M. Song, P. Purnell, I. Richardson*	73

Admixtures

D1	Effect of Acetic Acid on Early Hydration of Portland Cement *D.D. Nguyen, P. Koshy, C.C. Sorrell, L.P. Devlin*	75
D2	Impact of Polycarboxylate Superplasticizers on Polyphased Clinker Hydration *D. Marchon, M. Jachiet, R.J. Flatt, P. Juilland*	79
D3	Combined Effect of Malic Acid Retarder and Naphthalene Superplasticiser on Rheological Properties and Compressive Strength of NaOH-Activated Slag *J. Ren, I. Talagala, V. Kulasingham, Q. Zhou, Y. Bai, M.J. Earle, C.H. Yang*	83
D4	Future Challenges for Photocatalytic Concrete Technology *A. Folli, D.E. Macphee*	87
D5	The Influence of Sodium Salts and Gypsum on C-S-H *B. Mota, K. Scrivener, T. Matschei*	93
D6	Optimisation of Cement Grouts and CEM Mortars Using Different Superplasticisers, Mineral Additions and Supplementary Cementitious Materials *S. McNamee, M. Sonebi, S.E. Taylor*	99

Hydration and non-Portland binders

E1	*In situ* Monitoring of pH Changes in Concrete and Lime Mortars *G.L. Pesce, R.J. Ball, M. Serrapede, G. Denuault*	105
E2	Chemical Structure and Morphology of C-S-H Synthesized by Silica-Lime Reaction and by the Controlled Hydration of C_3S *E. Tajuelo Rodriguez, I. G. Richardson, L. Black, A. Nonat, J. Skibsted, E. Boehm-Courjault*	109

E3	Hydration of a High Equivalent Alkalis Clinker in the Presence of Natural and Synthetic Gypsum (Phosphogypsum) *L.S. Girotto, E.D. Rodríguez, F.A.L. Sánchez, A.P. Kirchheim, S.A. Bernal, J.L. Provis*	113
E4	Cement Pastes at the Nano-Scale: Opportunities from Modelling and Simulation *E. Masoero*	117
E5	Expansion Properties of Two Different Reactivity MgOs Produced from Magnesite and Seawater *W. Y. Lau, L. Mo and A. Al-Tabbaa, J. Stehle*	121
E6	Novel Process for Calcium Sulfoaluminate Cement Production *I. Galan, F.P. Glasser, A. Elhoweris, S. Tully, A. Murdoch*	125

Supplementary Cementitious Materials

F1	Development of an Electrical Leaching Technique - Evaluation of Leaching from Hardened Cement Body *K. Hashimoto, H. Yokota, H. Kinoshita, W. Gashier, A. MacArthur*	129
F2	Study of the Behavior of Resins Saturated with Na^+ ions in CEM I and CEM III Cement Pastes *E. Lafond, C. Cau Dit Coumes, D. Chartier, S. Gauffinet, A. Nonat, P. Le Bescop, L. Stefan*	133
F3	Microstructure and Phase Assemblage of Low-Clinker Cements during Early Stages of Carbonation *J. Herterich, L. Black, I. Richardson*	137
F4	Ultra-Fine Fly Ash Concrete *B.K.T. Kandie, K. Pilakoutas*	141
F5	Dissolution of Aluminosilicate Glasses in OPC environment *S. Alahrache, B. Lothenbach, F. Winnefeld, G.Accardo, J-B. Champenois, F. Hesselbarth*	147
F6	The Alumino-Silicate Chain Structure of C-S-H Phase in High-Volume Volcanic Natural Pozzolan-Portland Cement Blended Systems *A. Sassani, L. Turanli and C. Meral, A.H. Emwas*	151
F7	Pozzolanic Potential of the Calcined Clay-Lime System *S. Hollanders, J. Elsen*	155
F8	Effect of Cement Replacement by Limestone on the Hydration and Microstructural Development of Ultra High Performance Concrete *W. Huang, H.K. Kamyab, K. Scrivener, W. Sun*	159

Low CO_2 Cements and Concretes

G1	Improving the Carbonation Potential of MgO-Cement Porous Blocks through Different Aggregate Profiles *C. Unluer*	165
G2	Project Aether: Testing the Durability of a Lower-CO_2 Alternative to Portland Cement *K.C. Quillin, A.M. Dunster and C. Tipple, G. Walenta, E. Gartner, B. Albert*	169
G3	Towards the Development of CO_2-Neutral Cement (BioCement) *N.N. Carr, H.M. Jonkers*	173

Alkali-Activated and Other Cements

H1	Use of Magnesia Cement in Industrial Waste Cementation *Th. Zampetakis, H. Yiannoulakis and A. Meidani, A.I. Zouboulis, O. Zebiliadou, E. Pantazopoulou*	179
H2	Resistance against Organic Acid Attack in Fodder Fermenting Silo – Comparison of the Performance of OPC and Alkali-Activated Binder Based Concretes *A. Buchwald, P. Harpe, S. Schiecke, T. Hagedorn, B. Leydolph*	183
H3	Evaluation of Northern Irish Laterites as Precursor Materials for Geopolymer Binders *J. A. McIntosh, J. Kwasny, M. N. Soutsos*	187
H4	Durability Test Methods and their Application to AAMs: Acid Resistance *J. Aliques-Granero, T. M. Tognonvi, A. Tagnit-Hamou*	193
H5	Hybrid Organic-Inorganic Materials: Novel Perspectives for the Application of Geopolymer Based Materials *G. Roviello, L. Ricciotti, C. Ferone, F. Colangelo, R. Cioffi, O. Tarallo*	199
H6	Alkali-activated Slag Cements: Blast Furnace versus Ferronickel Slag *A. Fernández-Jiménez, K. Arbi, A. Palomo*	203
H7	Re-use of Waste Glass as Alkaline Activator in the Preparation of Alkali-Activated Materials *M. Torres-Carrasco, F. Puertas*	207

Poster Extended Abstracts

P1	Performance at high temperatures of alkali-activated slag/phlogopite binders *O.H. Hussein, S.A. Bernal, J.L. Provis*	211
P2	Utilization of High Volume Fly Ash Concrete With Indonesian Blended Cement as an Applicable and Environmentally Friendly Technology *R. R. Irawan*	217
P3	The CNASH_ss Thermodynamic Model: Formulation and Validation *R. J. Myers, S.A. Bernal, J.L. Provis*	221
P4	Thermal Insulation Rubber-Concrete for Building Walls Application *S.Y. Mukaila, A. Ocholi, S.P. Ejeh*	225
P5	Foamed Concrete: From Weakness to Strength *A.A. Hilal, N.H. Thom, A.R. Dawson*	231
P6	Optimising Blends of Blast Furnace Slags for the Immobilisation of Nuclear Waste *R.A. Sanderson, J.L. Provis, G.M. Cann*	235
P7	Hydration and Mechanical Properties of Portland Cement Blended with low-CaO Steel Slag *E. Atiemo, K.A. Boakye, J. Sarfo-Ansah*	237
P8	Effects of Blast Furnace Slag Substitution in Geopolymer Concrete on Compressive Strength and Corrosion Rate of Steel Reinforcement in Seawater And Acid Rain *H.W. Ashadi, S. Astutiningsih, B. A. Aprilando*	241

P9	Study of Blended Cement Matrices Containing Forest Biomass Ash *I. Jiménez, E. Puch, G. Pérez, A. Guerrero, B. Ruiz*	245
P10	Durability evaluation of an activated hybrid cementitious system using Portland cement and fly ash with Na_2SO_4 *D.F. Velandia, C.J. Lynsdale, J.L. Provis, F. Ramirez, A. Gomez*	249
P11	Phase Assemblages in Hydrated Calcium Sulfoaluminate Cements Blended with Mineral Additions *F. Winnefeld, B. Lothenbach*	253
P12	Cold-Setting Cordierite and Mullite-Cordierite Geopolymer Refractory Composites: Thermal Behavior, Mechanical Properties and Microstructure *C. N. Djangang, P. Mustarelli, E. Kamseu, C. Leonelli*	257
P13	Evaluation of Novel Reactive Mgo Activated Slag for the Immobilisation of Zinc *F. Jin, A. Al-Tabbaa*	261
P14	Influence of Variation in Chemical Composition on the Performance of Slag Blends in Chloride-Rich Environments *O.R. Ogirigbo, L. Black*	265
P15	On-Site (In-situ) Concrete Waste Minimisation in Tehran *A. Meibodi, H. Kew*	269
P16	Development of Self-cured Geopolymer Cement *T. Suwan, M. Fan*	273
P17	Atmospheric Scanning Electron Microscopy (ASEM) *In-Situ* Imaging of Microstructure Development in Hardening Cement Pastes *T. Takahashi, M. Kimura, T. Jinnai, H. Nishiyama*	277
P18	Influence of Blast Furnace Slag and Silica Fume on Early Age Engineering Performance of Alkali Activated Fly Ash after Short-Term Low Temperature Curing *F. Messina, C. Ferone, F. Colangelo, R. Cioffi*	279
P19	Microstructure-based Micromechanical Model for Compressive Strength Evolution of Cement Paste *M. Hlobil, V. Šmilauer*	283
P20	Concrete and Mortar Made with Incinerator Fly Ash *A.Y. Shebani*	287
P21	A New Binder from the Alkali Activation of Ceramic Sanitary-ware Waste *L. Reig, L. Soriano, M.V. Borrachero, J. Monzó, J. Payá*	291
P22	Chloride Binding Capacity of GGBS-based Cementitious Materials as Enhanced by Nano-alumina Addition *K. Briki, A. Darquennes, M. Chaouche*	295
P23	Early Hydration of OPC with Lignosulfonate *T. Danner, H. Justnes, M.R. Geiker*	301
P24	On the Optimum Sulphate Dosage: Study of the Model System C_3S/C_3A Ground with Hemi-Hydrate and Gypsum *S. Gauffinet, S. Gunay, A. Nonat, P. Temkhajomkit*	303
P25	Role of Ground Granulated Blast Furnace Slag on Sulphate Resistance *M. Whittaker, L. Black, M. Zajac, M. Ben Haha*	307
P26	Effect of Improper Curing on Concrete Performance *O. Idowu, L. Black*	311

P27	Effect of Temperature and Slag Properties on Slag/Cement Blend Hydration at Early Age *A. Bougara, C. Lynsdale, N. Milestone*	315
P28	Slag Hydration in Composite Cements *S. Adu-Amankwah, L. Black, M. Zajac*	321
P29	Comparison of X-ray Diffraction Rietveld Analysis and X-ray Fluorescence Bogue Analysis of Portland Cement Composition *G.M. Cann, I.H. Godfrey, R.M. Orr, R. Blackham, S. Foster*	325
P30	Factors Affecting the Properties of Na_2CO_3-activated Fly Ash/Slag Paste *A. Abdalqader, A. Al-Tabbaa*	329
P31	Thermal Behavior of Lightweight Aggregate Containing Mortar Subjected to Supercritical Carbonation *R.A.M. Júnior, J. M. Gurgel, M.R.F. Lima Filho, S.M. Torres, L. Black*	333
P32	Microstructure of Metakaolin Geopolymer Composite Subjected to Direct Flame *G. de S. Lima, K.C. Gomes , A.P. Vieira, M.R.F. Lima Filho, A.F. Leal, S.M. Torres*	337
P33	Alkaline Activation of Sugar Cane Bagasse Ashes *P.F. Filho, K.C. Gomes, J.F. Silva Neto, M.R.F. Lima Filho, S.M. Torres, A.P. Vieira*	341
P34	Development of Supplementary Cementitious Materials from London Clay *D. Zhou, C.R. Cheeseman, M. Tyrer*	345
P35	Alkali Activated Fuel Ash and Slag Mixes: Optimization Study from Mortars to Concrete Building Blocks *A. Rafeet, R. Vinai, W. Sha, M. Soutsos*	349
P36	High Performance Concrete Application using Recycled Aggregate and Synthetic Macro Fibre *A.I. Tijani, J. Yang, S. Dirar*	355
P37	Geopolymers based on Calcined Kaolin sludge/ Bottom Ash Blends and an Alternative Sodium Silicate Activator *M.A. Longhi, F. Gaedke, E.D. Rodríguez, A.C. Passuello, A.P. Kirchheim, S.A. Bernal, J.L. Provis*	359
P38	Impact of Mixing in the Early Hydration of Cement Paste with Lignosulphonate *A. Colombo, T.A. Danner, K. De Weerdt, M.R. Geiker, H. Justnes*	363
P39	Retarding Effect of Gluconate and D-Glucitol on the Hydration of Tricalcium Silicate: Interaction between the Molecules and Calcium Silicate Hydrates *C. Nalet, A. Nonat*	367
P40	Prediction of Drying Shrinkage and Compressive Strength of Self-Compacting Concrete using Artificial Neural Networks *J. Abdalhmid, M. Mahgub, A.F. Ashour, D. Lam, T. Sheehan*	371
P41	Study of the Hydration of Cement with High Slag Content *S. Stephant, L. Chomat, A. Nonat, T. Charpentier*	377
P42	High Temperature Study of FA/MKPC Binders for Nuclear Waste Encapsulation *L. J. Gardner, V. Lejeune, C.L. Corkhill, S.A. Bernal, J.L. Provis, N.C. Hyatt*	381

P43	The Hydration of Nuclear Wasteform Cements *J.E. Vigor, S.A. Bernal, I.H. Godfrey, J.L. Provis*	387
P44	Geopolymer from Mechanically Activated Low and High Calcium Fly Ash *G. Mucsi, Z. Molnár, Á. Rácz, R. Szabó, B. Csőke*	391
P45	Sodium Carbonate Activated Slag Binders for the Immobilisation Of Magnox Nuclear Waste *S.A. Walling, S.A. Bernal, N. C. Collier, H. Kinoshita, J.L. Provis*	397
P46	Early Stages of Aluminosilicate Glass Dissolution *K.C. Newlands, D.E. Macphee*	401
P47	How to Stabilize Spreader Stoker Coal Fly Ashes? *J. Hot, M. Sow, C. Tribout, M. Cyr*	407
P48	Influence of Graphene Oxide on the Hydration of Portland Cement: a preliminary investigation *S. Ghazizadeh, P. Duffour, Y. Bai, N.T. Skipper, M. Billing*	411
P49	Dielectric Properties and Numerical Modelling of Microwave Heating of Portland Cement/Fly Ash Blends *A. Khoylou, M. Debs, S. Shi, Y. Bai, M. Fabian, T. Sun, K.T.V. Grattan, B. McKinnon*	415
P50	Microwave Curing Techniques for Manufacturing Alkali-activated Fly Ash *S. Shi, Y. Bai, M. Fabian, M. Ams, T. Sun, K.T.V. Grattan, H. Li, D.L. Xu, P.A.M. Basheer*	419
P51	Chloride Binding Capacity of Hydrotalcite in Near-Neutral and Alkaline Environments *X. Ke, S.A. Bernal, J.L. Provis*	423
P52	Use of Oil-Based Mud Cutting waste in Cement Clinker Manufacturing *H. Saif Al-Dhamri, L. Black*	427
P53	Synthesis of Low-Energy Cement based on α-C_2SH *R. Siauciunas, K. Baltakys, R. Gendvilas, E. Prichockiene*	431
P54	Autogenous Shrinkage in Blended Cement Systems *Z. Hu, H. Kazemi-Kamyab, K. Scrivener*	435
P55	Nano-Structured SiO_2 Filler Made from Local Kuwaiti Sand and Used in Cement Paste Mixtures *S. Al-Otaibi, M. Sherif El-Eskandarany*	439
P56	Effect of Ca and Mg Addition on the Aqueous Durability of Glasses in High-pH Environments *D.J. Backhouse, C.L. Corkhill, N.C. Hyatt, R.J. Hand, M.L. Harrison*	443
P57	The Use of Urban Ceramic Wastes in Eco-Sustainable Durable Cement *V. Perugini, E. Paris, G. Giuli, M.R. Carroll*	447
P58	Natural Hydraulic Limes for Masonry Repair: Hydration and Workability *P.F.G. Banfill, A.M. Forster, S. MacKenzie, M. Pinilla Sanz, E.M. Szadurski, C. Torney*	451
P59	Formate Oxidation Driven Biogenic Concrete Surface Treatment by *Methylocystis Parvus* OBBP *G. Ganendra, J. Wang, A. Ho, N. Boon*	455

P60	Impact of High Temperature to Aluminous Cement Based Fibre Composites Containing Polycarboxylate Superplasticizer *P. Reiterman, M. Jogl, O. Holčapek, J. Litoš, P. Máca, R. Sovják, P. Konvalinka*	459
P61	Reutilization of Clay Brick Aggregate and Powder Derived from Construction and Demolition Waste in Concrete *S.C. Kou, F. Xing, C.S. Poon*	463
P62	Effect of $CsNO_3$ on 3:1 Blast Furnace Slag:Portland Cement Systems *A.J. MacArthur, H. Kinoshita, J.L. Provis, S. Shaw*	467
P63	Early-age Engineering Properties and Electrical Resistivity of Geopolymer Mortars *X. Zhou, S. Safari*	471
P64	A New Method for Assessment of Cracking Tendency of Cement-based Materials under Restrained Shrinkage *X.M. Zhou, O. Oladiran, W. Dong*	473

Workshop on Waste Cementation – 17 Sep 2014

Oral Session Extended Abstracts

W1	***Keynote* - Immobilisation of Intermediate Level Waste Using Cements – Research Progress and Future Opportunities** ***M. Angus***	**477**
W2	***Keynote* - Cement Matrices for Nuclear Waste Immobilisation – Recent Advances** ***J.L. Provis, S.A. Bernal, C. Corkhill, H. Kinoshita, N.C. Hyatt***	**479**
W3	Magnesium Silicate Hydrates (M-S-H): Formation Kinetics and Range of Composition *E. Bernard, B. Lothenbach, E. L'Hôpital, D. Nied, A. Dauzères*	481
W4	Magnesium and Calcium Silicate Hydrates *B. Lothenbach, E. L'Hôpital, D. Nied, G. Achiedo, A. Dauzères*	485
W5	Gamma Radiation Resistance at Early Age of a Slag-Portland Cement Binder Used for the Treatment of Nuclear Waste *N. Mobasher, S. A. Bernal, H. Kinoshita, C.A. Sharrad, J.L. Provis*	489
W6	Reactivity Testing of Ground Granulated Blastfurnace Slag and Fly Ash *G.M. Cann, K. Carruthers, I.H. Godfrey, S. Foster, K. Murphy*	493
W7	Performance of Portland Cement Pervious Concrete In Removal Process of Heavy Metals from Stormwater *A. Abdollahzadeh*	495
W8	Immobilisation of Technetium-99 on Backfill Cement: Sorption under Static and Saturated Flow Conditions *C.L. Corkhill, J.W. Bridge, P. Hillel, L.J. Gardner, R. Tappero, N.C. Hyatt*	497
W9	High-Resolution Multi-Nuclear NMR Characterisation of a Novel GBFS/MKPC Binder for Nuclear Waste Encapsulation *L.J. Gardner, S.A. Bernal, S.A. Walling, C.L. Corkhill, J.L. Provis, N.C. Hyatt*	499

W10	Determination of the Extent of Expansion of Residual Metallic Waste and its Effect on ILW Containers *M. Hayes, S.J. Palethorpe, G.R. Patterson, G. Woodhouse*	503
W11	Potential Use of Cementation of Copper Tailing for Infrastructure Development in Papua *R.R. Irawan, S. Hardono, R. Wijaya, F. Yuliarti, N. Visco, F. Mulyana*	507
W12	MSWI Fly Ash Cementation by Means of Cold-Bonding Pelletization *F. Colangelo, C. Ferone, F. Messina R. Cioffi*	511
W13	***Keynote* - Stabilization of Textile Effluent Sludge for Producing Concrete Blocks** ***C.S. Poon, B. Zhan***	**515**
W14	Induced Cementation of Dredged Marine Soils for Civil Engineering Re-Use *C-M. Chan*	519
W15	Effect of Composition on Laser Scabbling of Cementitious Materials in Nuclear Decommissioning *B. Peach, M. Petkovski, D.L. Engelberg, J. Blackburn*	523

Poster Extended Abstracts

W16	Study for Utilization of Industrial Solid Waste, Generated by the Discharge of Casting Sand Agglomeration with Clay, Blast Furnace Slag and Sugar Cane Bagasse Ash in Concrete Composition *J. Mazariegos Pablos, E.P. Sichieri, M. S. de Andrade Zago*	525
W17	Cementitious Grouts for ILW Encapsulation – Continuity of Supply/Influence of Organic Grinding Aids *J. Hawthorne*	527
W18	Assessment of the Hydrothermal Ageing of Waste Encapsulation and Backfill Grouts for Applications in the Nuclear Industry *E.J. Butcher, N. Collier, K. Carruthers, J. Borwick, S.J. Williams*	529
W19	Magnesium Aluminium Silicate Hydrate (M-A-S-H) Cements for Magnox Sludge Immobilisation *S.A. Walling, S.A. Bernal, H. Kinoshita, J.L. Provis*	531
W20	Biomass Fly Ash as a Precursor for Alkali-Activated Materials *S.A. Bernal, S. Mundra, O.H. Hussein, R.J. Ball, A.C. Heath, J.L. Provis*	535

34th Cement and Concrete Science Conference
14-17 September 2014
University of Sheffield

In situ Monitoring of pH Changes in Concrete and Lime Mortars

G.L. Pesce, R.J. Ball
BRE Centre of Innovative Construction Materials, Department of Architecture and Civil Engineering, University of Bath, Bath, BA2 7AY

M. Serrapede, G. Denuault
Department of Chemistry, University of Southampton, Southampton, SO17 1BJ

ABSTRACT

This paper describes how a new type of solid state microelectrode based on nanostructured palladium-hydride (PdH) can be used to monitor pH variations during carbonation of calcium hydroxide ($Ca(OH)_2$). The experiments described were carried out under conditions similar to those typical of common porous substrates such as cement and lime mortars. In these tests PdH microelectrodes were employed to record pH transients during the carbonation within a humid fibrous mesh that simulated the porous substrate. To control the carbonation rate, experiments were carried out at different carbon dioxide partial pressures (p_{CO2}) and in each case the experimental results were compared to theoretical calculations obtained using PHREEQC (pH-REdox-EQuilibrium) software. Scanning electron microscopy (SEM) observations and X-ray diffraction (XRD) analysis of the calcium carbonate ($CaCO_3$) crystals deposited on the fibrous mesh were used to evaluate characteristics of the solid phases precipitated during the reaction. Results demonstrate that these pH microsensors can operate reliably in very alkaline environments (pH>12) such as those produced by the dissolution of $Ca(OH)_2$.

1. INTRODUCTION

One of the most important electrochemical measurements is that of the acidity or basicity of aqueous solutions. Numerous chemical reactions involve pH changes that can highlight processes otherwise difficult to monitor such as the corrosion of steel bars in reinforced concrete.

The steel reinforcement in concrete is normally in a passive state with respect to corrosion due to a thin iron oxide layer produced by the highly alkaline environment (pH>12) of the concrete pore solution. This alkaline environment is mainly produced by the $Ca(OH)_2$ contained in the cement as well as by the smaller amount of other alkaline species such as sodium and potassium hydroxides (NaOH and KOH, respectively) [1].

Because of the reduced porosity of concrete, these hydroxides do not fully carbonate during the hardening process and this guarantees an almost constant alkaline environment that maintains the protective layer around the steel reinforcement preventing corrosion [2]. However, over time CO_2 may penetrate within the concrete and cause carbonation of alkali and alkaline-earth elements. This eventually produces a more acidic environment which reduces the passive iron oxide layer and increases the risk of corrosion of the underlying steel. For this reason monitoring the pH of pore waters in steel reinforced concrete structures is key to assessing the state of the structures [3].

Despite its importance pH remains a difficult parameter to determine in many applications, including those in the construction industry. In this specific case, two of the main factors affecting pH measurements are: (1) pHs above 11 cannot be measured reliably with most of the currently used pH sensitive devices including the conventional glass electrode, because of the alkaline error; (2) pH is hard to measure in confined places. The alkaline error is due to the fact that in high pH solutions (>11) the hydrogen ion activity is so low and the activity of alkali or alkaline-earth metal ions (mainly contained in the glass of the membrane) is so high that the ordinary pH electrode begins to respond to these ions rather than to the hydrogen ions. To take this effect into account correction tables are available as well as special electrodes (although the correction tables are preferred, [3, p.126]). These special electrodes use alkali-glass membranes that are less sensitive to ions such as Na^+ and Li^+. However, none of the glass membranes currently available has zero alkaline error [4]. For instance, the Sentek P11-PB (PH0043) combination type electrode, sold as suitable for measurements within the pH

range 0-14 and, in particular, for measuring the pH in cement, returned a pH of 12.8 in a pure $Ca(OH)_2$ aqueous solution whose pH at 20ºC, according to theoretical calculations and to some measurements carried out with a solid state electrode, had to be 12.56.

2. A NEW WAY OF MONITORING pH IN BUILDING MATERIALS: THE NANO-STRUCTURED PdH MICROELECTRODES

In order to overcome limitations of traditional pH electrodes, a new type of electrode can be exploited for monitoring pH variations in cement and lime mortars: *the nano-structured PdH microelectrode.*

This solid state electrode operates by exploiting the insertion of hydrogen in the palladium (Pd) structure. This absorption leads to a phase change by forming palladium hydride (PdH).

The maximum amount of hydrogen that can be absorbed within the Pd film is relatively large (up to 0.6 H per Pd atom). The crystalline structure formed is dictated by the quantity of H absorbed. Two phases are obtained: the α phase, when the H:Pd ratio is below 0.02, and the β phase when the ratio is above 0.6 In between these limits, the PdH consists of a mixture of the two phases [5, p.8341]. Under these latter conditions, the PdH behaves as a hydrogen electrode yielding a Nernstian dependence of potential on pH, independent of the Pd:H ratio.

Despite the publication of extensive studies of H insertion / extraction in Pd, only one report was published in 2006 regarding a PdH micro-pH sensor [6, p.266]. This was probably due to the fact that the potentiometric response of PdH microelectrodes is generally worse than that of large PdH electrodes. Generally the smaller the electrode, the more unstable is its potentiometric response.

However, the nanostructure introduced in 2006 by Imokawa and colleagues avoids these problems [6, p.266] and allows the PdH micro-electrodes to be successfully used in a number of applications. The nanostructure, in fact, increases the H absorption rate and allows a rapid, stable, reproducible and almost theoretical potentiometric pH response in de-aerated solutions. Furthermore, thanks to these characteristics, the electrode can be reloaded with hydrogen quickly, thereby allowing repeated pH measurements [6, p.271].

3. MONITORING pH IN BUILDING MATERIALS WITH NANOSTRUCTURED PdH MICROELECTRODES

To demonstrate the reliability of these electrodes in monitoring pH variation in porous building materials some tests were carried out in a joint research project between the University of Southampton and University of Bath (UK).

In this research, carbonation was studied within a thin film of water to simulate the conditions existing in a porous media such as concrete once most of the liquid water has evaporated. Experiments were carried out in a specifically constructed PMMA cell under thermostatic conditions (23°C) with different $Ar:CO_2$ gas mixtures. The saturated solution of $Ca(OH)_2$ used for the tests was absorbed onto small strips of cotton lint (3mm wide, 10mm in length) wrapped around the reference electrode. This cotton mesh was used to trap a thin film of solution and simulate carbonation in the confinement of a porous medium, as well as provide an ionic path between the electrodes and capture the solid phases formed during the carbonation for subsequent analysis.

To control the carbonation, the experiments were carried out at different p_{CO2} and in each case the experimental results were compared to theoretical calculations using PHREEQC. The micro-morphology and crystalline structure of solid phases precipitated on the mesh fibres during the tests were studied using a field emission scanning electron microscope (model FESEM6301F from JEOL) and an X-ray diffractometer (Rigaku Smartlab with a 9 kW source and CuK_α X-rays).

Tests were carried out using a three-electrode configuration consisting of the PdH micro-electrode (a 250µm diameter, 2µm thick disc of nanostructured Pd electrodeposited on a Pt disc as reported in [6]), a platinum mesh counter electrode and a saturated calomel reference electrode. The microelectrode was held by a translation stage and inserted in the cell through a specifically made hole in the cell lid. The Pt mesh was clamped at the bottom of the cell by the cell lid and the reference electrode was clamped outside the cell and connected to the solution by means of a salt bridge. The latter was terminated by a capillary tip attached to the microelectrode and held circa 2mm away.

In order to evaluate the Pd microelectrode response, the pHs obtained at the beginning and end of the tests were compared with theoretical values calculated following previously reported PHREEQC (a program for simulating homogeneous and heterogeneous geochemical reactions) protocols [7]. The initial condition was for a solution consisting of 1 kg of pure water with the addition of sufficient Ca^{2+} ions to simulate saturation with lime at temperatures of 20, 23 and 25°C. The equilibrium phases considered for evaluating the final pH were: gaseous CO_2 at different

partial pressures and one of the solid polymorphs of $CaCO_3$. The partial pressure of CO_2 considered was the same used during all the experiments. The number of moles of CO_2 was set to 1000 in order to model the equilibrium with an effectively infinite reservoir. Solid $CaCO_3$ phases introduced into the simulation were: monohydrocalcite, vaterite, aragonite and calcite. These were introduced using a saturation index of zero. Simulations were performed with the thermodynamic data contained in the Lawrence Livermore National Laboratory database which was modified by adding data for vaterite taken from the SIT database, developed for the French National Radioactive Waste Management Agency.

Table 1. Initial and final pH values calculated with PHREEQC for the carbonation of a saturated $Ca(OH)_2$ solution at different temperatures and p_{CO2} (In pH=initial pH; Mon=monohydrocalcite; Vater= vaterite; Arago=aragonite; Calc=calcite)

T (°C)	In. pH	p_{CO2} (atm)	Final pH			
			Mon	Vater	Arago	Calc
20	12.56	0.750	6.389	6.317	6.139	6.087
		0.167	6.805	6.734	6.559	6.508
		0.039	7.215	7.154	6.972	6.921
23	12.45	0.750	6.338	6.310	6.135	6.083
		0.167	6.805	6.728	6.555	6.504
		0.039	7.214	7.139	6.968	6.917
25	12.37	0.750	6.388	6.306	6.132	6.080
		0.167	6.805	6.724	6.553	6.501
		0.039	7.214	7.135	6.996	6.915

4. EXPERIMENTAL RESULTS

Table 1 reports the initial (second column) and final pH (last four columns) of a saturated $Ca(OH)_2$ solution before and after carbonation at different temperatures and p_{CO2} as calculated by PHREEQC.

Figure 1 shows the potential transient (left axis) measured by the electrode during carbonation of the solution at 23°C and 0.167atm p_{CO2}. The pH values reported on the right axis were calculated from the potential transient using the potential-pH calibration curve published in [8] where the slope, 58.7±0.5 mV/pH, was in good agreement with the slope found previously by Imokawa and colleagues [6].

For the first 27 min, figure 1, the cell was full of solution and the microelectrode measured the potential in the bulk solution. During this time an inert atmosphere of Ar was introduced into the cell to prevent carbonation. A rise in potential within the first 20 minutes reflected the loss of hydrogen from the β phase of the PdH. Between 20 and 45 minutes a plateau appeared when the α phase started to form. This effect lasted while the two phases coexisted. Under this condition the electrode potential was only determined by the pH allowing the micro-electrode to act as a pH electrode.

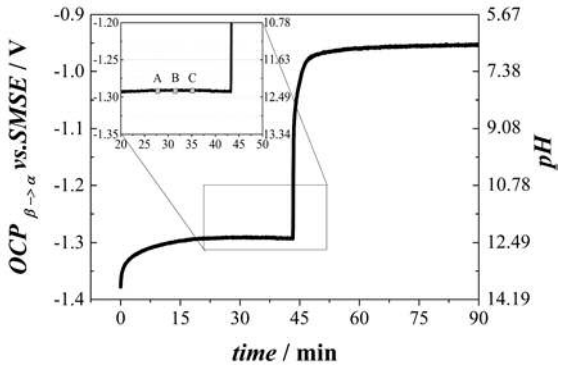

Figure 1. Potential transient (left axis) and corresponding pH (right axis) recorded with a 250 µm diameter nano-structured PdH microelectrode during the carbonation of a saturated $Ca(OH)_2$ solution at 23°C and 0.167 atm p_{CO2}.

After about 27 minutes from the beginning of the experiment, when the bulk measurement was considered stable, the microelectrode was moved down toward the cotton lint (point A in the inset in figure 1). Once in contact, the signal stability was checked and, then, the solution was removed using a syringe connected to a capillary tube (point B in figure 1). After having checked once again the stability of the potential transient, a mixture of Ar and CO_2 with a p_{CO2} of 0.167atm was introduced into the cell (point C). Soon after, the potential began to rise steeply until it reached a second plateau. This steep increase reflected the change in pH due to the carbonation reaction within the solution trapped in the mesh. A new plateau was reached after approximately 60 minutes from the beginning of the experiment. This reflected the potential (i.e. the pH) of a theoretical water solution with no free Ca^{2+} ions, in equilibrium with two phases: a $CaCO_3$ solid phase and CO_2 gaseous phase. At this stage all Ca^{2+} ions initially in solution were bonded to CO_3^{2-} ions in the $CaCO_3$ structure and the pH was mainly influenced by the solubility of the solid phases formed and by the p_{CO2} (table 1).

According to the calibration curve in [8], the initial pH of the solution was 12.45 (between points A and C in figure 1). A value in perfect agreement with the results of the PHREEQC calculation (table 1) and quite different from the values measured with the glass electrodes in a similar solution (about 12.7). In comparison, the pH of the plateau formed at the end of carbonation was 6.34. The theoretical pH of a similar system calculated by PHREEQC, assuming formation of calcite, was 6.50 (table 1). Repetitions of the same test (table 2) led to a mean experimental value of 6.46±0.06. The

difference between this mean and the theoretical value (-0.04) suggests that calcite is the most likely phase formed. To ascertain which phase had precipitated, the mesh was observed using a SEM.

Table 2. Experimental pH values recorded at the end of the carbonation tests of a saturated $Ca(OH)_2$ water solution at different p_{CO2} and at 23°C.

p_{CO2} (atm)	1st test	2nd test	3rd test	average	St. Error
0.750	6.13	6.06	6.17	6.12	0.03
0.167	6.34	6.56	6.47	6.46	0.06
0.039	6.95	6.78	6.85	6.86	0.05

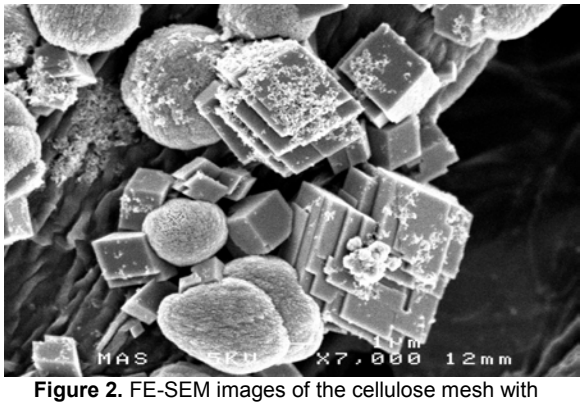

Figure 2. FE-SEM images of the cellulose mesh with calcite. The sample was previously coated with chromium to avoid charging in the SEM chamber.

Figure 2 shows the morphologies of the main solid phase found on the cotton lint. The rhombohedral crystals are characteristic of calcite formations while the round particles among some of the rhombohedra are characteristic of vaterite. Results of the SEM analysis were confirmed by X-ray diffraction. More details on these tests and the results obtained are reported in [8].

5. CONCLUSIONS

This study demonstrates that pH micro-sensors manufactured from nano-structured PdH can operate reliably in very alkaline environments such as those produced by the dissolution of $Ca(OH)_2$. The electrodes were successfully employed to monitor the pH changes during carbonation in a porous substrate exposed to different p_{CO2} and the pH detected in situ was found to be in perfect agreement with the theoretical calculations made with PHREEQC. To our knowledge, these microelectrodes are currently the only analytical tool capable of monitoring high pH in confined places. For this reason these electrodes can be considered very valuable for the study of reactions involving building materials.

ACKNOWLEDGEMENTS

The authors would like to thank the Engineering and Physical Sciences Research Council (EPSRC) for financial support through projects EP/I001204/1, EP/J004219/1 and EP/K025597/1.

REFERENCES

[1] Garcia-Alonso M, Escudero M, Miranda J, Vega M, Capilla F, Correia M, Salta M, Bennani A, Gonzalez J, 2007. Corrosion behaviour of new stainless steels reinforcing bars embedded in concrete. *Cement and Concrete Research* 37(10), pp. 1463–1471.

[2] Bertolini L, Elsener B, Pedeferri P, Redaelli E, Polder R.B, 2013. *Corrosion of steel in concrete. Prevention, diagnosis, repair.* 2nd Edition. Wiley-VCN Verlag GmbH and Co.

[3] Pu Q, Jiang L, Xu J, Chu H, Xu Y, Zhang Y, 2012. Evolution of pH and chemical composition of pore solution in carbonated concrete. *Construction and Building Materials* 28(1), pp. 519–524.

[3] Garrels RM, Christ CL, 1965. *Solutions, minerals, and equilibria*. Freeman, Cooper & Company.

[4] Ives DJG, Janz GJ, 1961. *Reference electrodes: theory and practice*. Academic Press, New York-London.

[5] Serrapede M, Denuault G, Sosna M, Pesce GL, Ball RJ, 2013. Scanning electrochemical microscopy: using the potentiometric mode of SECM to study the mixed potential arising from two independent redox processes. *Analytical Chemistry*. 85(17), pp 8341–8346.

[6] Imokawa T, Williams KJ, Denuault G, 2006. Fabrication and characterization of nanostructured Pd hydride pH microelectrodes. *Analytical Chemistry*. 78(1), pp. 265–271.

[7] Appelo CAJ, Postma D, 2005. *Geochemistry, groundwater and pollution*. Taylor & Francis.

[8] Serrapede M, Pesce GL, Ball RJ, Denuault G, 2014. Nanostructured Pd Hydride Microelectrodes: In Situ Monitoring of pH Variations in a Porous Medium. Analytical Chemistry, 86(12), pp. 5758-5765.